A 6.78 MHz Multiple-Receiver Wireless Power Transfer System with Constant Output Voltage and Optimum Efficiency

Minfan Fu, *Member, IEEE,* He Yin, *Member, IEEE,* Ming Liu, *Member, IEEE,* Yong Wang, *Member, IEEE,* Chengbin Ma, *Member, IEEE*

***Abstract*—This paper develops a 6.78 MHz multiple-receiver wireless power transfer system driven by a Class E power amplifier. Constant output voltage is achieved for each receiver with optimized overall efficiency. A novel one-receiver model is built to analyze the overall power-efficiency characteristics. The loads and input voltage are then designed as two control variables. Through tuning the loads, constant output voltage is achieved by independent controllers at the receiver side. Then the efficiency is optimized by tuning the input voltage at the transmitter side. Finally, the theoretical analysis and control scheme are validated using a three-receiver system. It shows that different constant output voltages, 5 V, 9 V, and 12 V can be achieved independently for different receivers. When the load resistance, real coupling, and number of receivers change, the voltage can be quickly regulated, and the overall optimum system efficiency is 66.6%.**

***Index Terms*—Wireless power transfer, multiple receivers, class E power amplifier, constant output voltage, efficiency optimization**

I. Introduction

Wireless power transfer (WPT) has attracted an increasing attention among industrial and academic sectors. One of its unique advantages is to simultaneously charge multiple receivers (RXs), such as wearable devices, cellphones, and household appliances. At the same time, it also presents challenges on the system analysis and control, especially considering the change of coupling, loads, and number of receivers. Such issues have been well studied in the conventional one-RX systems. Examples of the efforts include the design of power amplifier (PA) and rectifier [1], [2]; analysis of coupling coils [3], [4]; tunable circuits [5]; and feedback-based control [6].

© 2017 IEEE. Personal use of this material is permitted. Permission from IEEE must be obtained for all other uses, including reprinting/republishing this material for advertising or promotional purposes, collecting new collected works for resale or redistribution to servers or lists, or reuse of any copyrighted component of this work in other works.

Manuscript received Feb. 16, 2017; revised May 19, 2017; accepted June 30, 2017. This work was supported by the Shanghai Natural Science Foundation under Grant 16ZR1416300.

M. Fu is with the Center for Power Electronics Systems, Virginia Polytechnic Institute and State University, Blacksburg, VA 24061, USA (e-mail: minfanfu@vt.edu).

H. Yin, M. Liu, and C. Ma are with the University of Michigan-Shanghai Jiao Tong University Joint Institute, Shanghai Jiao Tong University, 800 Dongchuan Road, Minhang, Shanghai 200240, China (e-mail: yyy@sjtu.edu.cn; mikeliu@sjtu.edu.cn; chbma@sjtu.edu.cn).

Y. Wang is with Department of Electrical Engineering, Shanghai Jiao Tong University, 800 Dongchuan Road, Minhang, Shanghai 200240, P. R. China (email: wangyong75@sjtu.edu.cn).

Parallel with the one-RX systems, many research groups have also shown strong interests in multiple-RX systems. Fundamental works were carried out to evaluate the power transfer characteristics between the coupling coils [7]–[9]. With these basic findings on coil performance, efforts are placed on developing practical systems by including more control freedoms and power stages. For example, multiple frequencies are used in [10]–[13] to charge several devices; Impedance matching networks are proposed to adjust the power distribution among RXs [14]–[16]; Additional coils can be used to manage the power flow among multiple RXs [17], [18]; Multiple-TX multiple-RX system configuration is also developed in [19]–[21]; Omni-directional power transfer is achieved by using three-dimensional coils and cavity [22], [23]. All these fundamental works show the variety of possible solutions for multiple-RX applications, and well contribute the progress on the research on multiple-RX systems. However, their ideas were validated by the open-loop measurements. In applications more practical issues should be considered, such as the output power regulation, efficiency optimization, control complexity, and hardware implementation. Furthermore, a multiple-RX system should work robustly under various uncertainties, which are mainly caused by the change of coupling, load resistance, and number of RXs. Therefore, it is important to develop a feedback-based system with a suitable design and control scheme.

In planar charging applications, it is practical to use single transmitter to charge multiple portable devices. A MHz WPT system is promising for such small-power applications thanks to its improved spacial freedom. A MHz system usually uses a Class E power amplifier (PA), i.e., dc/ac, to drive the TX coil due to the high efficiency of the PA. For each receiver, a rectifier and a dc/dc converter are respectively used for ac/dc conversion and control purposes (voltage regulation or efficiency optimization). This four-stage (dc/ac, ac/ac, ac/dc, and dc/dc) configuration has been adopted by the A4WP standard and applied in the control of WPT systems [24], [25]. In [24], the system efficiency is optimized to 71% based on a tracking mechanism. However, the output voltage is not regulated. Although the regulation of the output voltage is discussed in [25], the efficiency significantly varies from 66% to 48% under loading and coupling variations. For the four-stage configuration, new efforts are expected to simultaneously regulate the output voltage and optimize the efficiency.

The challenge mainly arises from the complicated relation-

ship between the output power and efficiency. They are closely coupled due to the load sensitive Class E PA. In order to simplify the control, in this paper, a new equivalent one-RX model is developed to investigate the power-efficiency characteristics of the overall system. All the changes in the coil coupling, load resistance, and number of RXs can be reflected in the developed one-RX model, namely with reduced complexity of the system modeling. Based on the one-RX model, the input resistance of the buck converters and the input voltage of the PA show the potential for improved power and efficiency control. In order to simplify the control complexity, a robust system design is proposed, which considers all kinds of variations. Then simple RX controllers are applied to regulate the output voltage independently. Finally, the minimum input voltage is tuned by the TX controller to optimize the overall efficiency. For both the RX and TX controllers, only dc signals are required in the feedback-based control. It is known that many mature dc/dc converters and control techniques are available to further improve the overall system efficiency. The proposed modeling, design, and control methodology can be easily implemented in the four-stage MHz system. It is particularly suitable for applications following the A4WP standard.

II. System Analysis and Modeling

A. System Configuration

The four-stage configuration is shown in Fig. 1. There are n RXs charged by a TX. The TX consists of a dc source, a Class E PA, and a TX coil; Each RX consists of a RX coil, a rectifier, a buck converter, and a final load. In this paper, i is used to denote different RXs. A RX controller is applied for each RX to ensure constant output voltage $V_{L,i}$, and there are totally n degree of control freedoms at the RX side. Generally, constant $V_{L,i}$ can be maintained if the input voltage V_{PA} is sufficiently large. However, a constant V_{PA} can lead to a low-efficiency system when under wide load range [25]. Therefore, a TX controller should be used to maintain high overall efficiency. There are mainly three tuning approaches, such as the frequency tuning, dynamic impedance matching, and input voltage regulation. Considering the narrow industrial scientific medical (ISM) band, a fixed frequency system is preferred for MHz WPT applications. Besides, it is usually unattractive to use the switch-based impedance matching network because the network requires complicated circuits and control algorithm with inevitable component loss [5], [16]. In this paper, the input voltage regulation is used for the efficiency optimization. It requires a front-stage converter to transform the ac voltage into a tunable V_{PA}, and a large amount of mature high-efficiency conversion circuits can be used. Thus this paper focuses on the power transfer from the PA to the final load. The proposed design and control methodology is valid for all front-stage converters.

The proposed control scheme uses $(n+1)$ control variables for $(n+1)$ objectives (i.e., constant $V_{L,i}$'s and maximum efficiency). Usually, these objectives are closely coupled through the load sensitive PA, which are much more complicated in a multiple-RX system. The main challenge is to develop suitable design methodology and control scheme to make sure different controllers can work independently. Therefore, it is necessary to investigate the power-efficiency characteristics under different loading and coupling conditions.

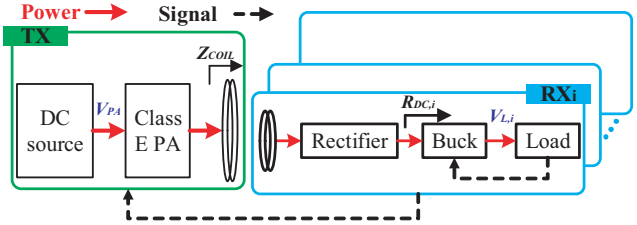

Fig. 1. Multiple-RX WPT system configuration.

B. PA's Output Characteristics

The system power-efficiency characteristics are mainly determined by the Class E PA. Its circuit model is shown in Fig. 2(a), where L_F is a radio frequency (RF) choke, S_1 is a transistor, C_S is a shunt capacitor, L_0 and C_0 forms a series resonant circuit with net reactance jX, Z_{COIL} $(= R_{COIL} + jX_{COIL})$ is the load of PA. In this circuit, V_{PA} and I_{PA} are the input voltage and current of the PA. The efficiency for the PA is

$$\eta_{PA} = \frac{P_{COIL}}{P_{PA}}, \tag{1}$$

where P_{PA} and P_{COIL} are the input and output power of the PA.

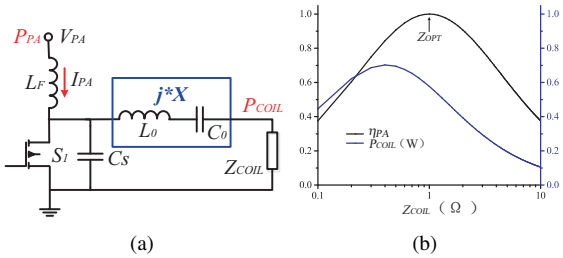

(a) (b)

Fig. 2. Class E power amplifier. (a) Circuit model. (b) Efficiency and output power using normalized parameters.

The parameters of the PA can be optimized for a target load Z_{OPT} by Raab's equations [26],

$$\begin{cases} B = \omega C_S = \frac{8}{\pi(\pi^2+4)Z_{OPT}} \approx \frac{0.184}{Z_{OPT}} \\ X = \omega L_0 - \frac{1}{\omega C_0} = \frac{\pi(\pi^2-4)Z_{OPT}}{16} \approx 1.15 Z_{OPT} \end{cases}, \tag{2}$$

where B is the susceptance of C_S at the working frequency ω. Using the optimized B and X, P_{COIL} and η_{PA} can be analytically derived for any Z_{COIL} =$(R_{COIL} + jX_{COIL})$ and V_{PA} [27],

$$\begin{cases} P_{COIL}(V_{PA}, Z_{COIL}) = \frac{V_{pa}^2 g^2 R_{coil}}{2R_{pa}^2} \\ \eta_{PA}(Z_{COIL}) = \frac{g^2 R_{coil}}{2R_{pa}} \end{cases}. \tag{3}$$

where

$$g = \frac{\pi \sin\phi_1 + 2\cos\phi_1}{2\cos\phi \sin\phi_1 + \pi/2 \cos\psi}, \tag{4}$$

$$R_{pa} = \frac{\pi^2/4 - g[\pi/2\cos\phi + \sin\phi]}{\pi B}, \tag{5}$$

$$\psi = \tan^{-1}\left(\frac{X+X_{coil}}{R_{coil}}\right), \tag{6}$$

$$\phi = \tan^{-1}\left[\frac{(\pi^2/2-4)-\pi B R_{coil}\rho(2\cos\psi+\pi\sin\psi)}{\pi+\pi B R_{coil}\rho(\pi\cos\psi-2sin\psi)}\right], \tag{7}$$

$$\phi_1 = \phi + \psi, \tag{8}$$

$$\rho = \sqrt{1+\left(\frac{X+X_{coil}}{R_{coil}}\right)^2}. \tag{9}$$

All the above variables, g, R_{pa}, ψ, ϕ, ϕ_1 and ρ, relate to the coil input impedance, Z_{coil}. Using normalized parameters, i.e., $V_{PA} = 1$ V and $Z_{OPT} = 1\ \Omega$, the power-efficiency characteristics of the PA are evaluated in Fig. 2(b). It shows the PA can achieve high η_{PA} around Z_{OPT}. Meanwhile both P_{COIL} and η_{PA} are sensitive to Z_{COIL} variation. Since Z_{COIL} is the overall loading effect caused by all RXs [refer to Fig. 1], it is the load sensitive PA that determines the complicated power-efficiency characteristics in multiple-RX applications. In this paper, all the changes of the load resistance, the coupling, and the number of RXs can lead to a varied Z_{COIL}, and are fully considered in the system-level analysis.

C. Multiple-RX WPT System

This paper is to develop a WPT system with one planar TX and multiple RXs. The RX coils are right above the TX coil with no overlap. The cross coupling effects between RX coils are avoided, and thus the effects are not discussed for the target planar charging application. Refs. [9], [24] discuss the compensation of the cross coupling and a control method when the cross coupling exists. The multiple-RX WPT system in Fig. 1 can be simplified as shown in Fig. 3. L, C and R with different subscripts represent coil inductors, compensated capacitors, and parasitic resistors of the TX and RX coils, receptively. M_{ti} is the mutual inductance between the TX coil and RX$_i$ coil. At the RX side, the circuit after the RX coil is equivalently represented by $Z_{REC,i}$. $\mathbf{M}$ and $\mathbf{Z_{REC}}$ represent the vectors for M_{ti}'s and $Z_{REC,i}$'s.

The resonance of the coupling coils is achieved by

$$j\omega L_t + \frac{1}{j\omega C_t} = 0 \text{ and } j\omega L_i + \frac{1}{j\omega C_i} = 0. \tag{10}$$

Under resonance, the reflected impedance of RX$_i$ on the TX side is

$$Z_{R,i} = \frac{\omega^2 M_{ti}^2}{R_i + Z_{REC,i}}, \tag{11}$$

and the coil input impedance is

$$Z_{COIL}(\mathbf{Z_{REC}}) = R_t + \sum_{i=1}^{n} Z_{R,i}. \tag{12}$$

The power transfer between the coupling coils can be described based on the power division law. At the TX side, P_{COIL} is first delivered to each $Z_{R,i}$ with losses on R_t.

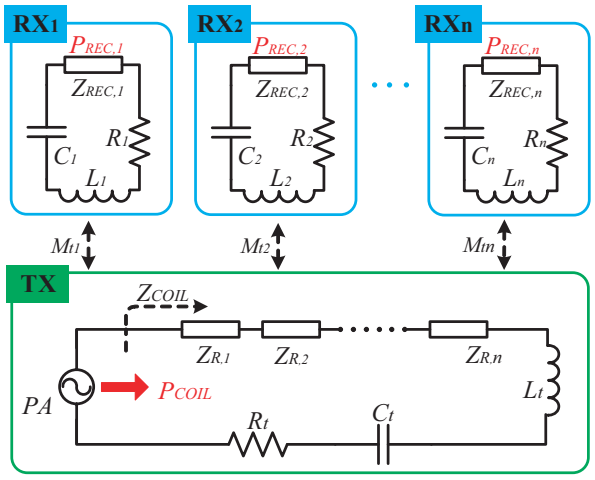

Fig. 3. Multiple-RX WPT system configuration.

Then at each RX side, the power received by $Z_{R,i}$ is further transferred to the corresponding $Z_{REC,i}$ with losses on R_i. Therefore, the power received by $Z_{REC,i}$ and the efficiency between the TX coil and the RX$_i$ coil are

$$\begin{cases} P_{REC,i}(V_{PA}, \mathbf{Z_{REC}}) = P_{COIL} \cdot \eta_{COIL,i} \\ \eta_{COIL,i}(\mathbf{Z_{REC}}) = \frac{Z_{R,i}}{Z_{COIL}} \cdot \frac{Z_{REC,i}}{R_i + Z_{REC,i}} \end{cases}. \tag{13}$$

Then the overall power received by $\mathbf{Z_{REC}}$ and the overall efficiency of the coupling coils are

$$\begin{cases} P_{REC}(V_{PA}, \mathbf{Z_{REC}}) = \sum_{i=1}^{n} P_{REC,i} \\ \eta_{COIL}(\mathbf{Z_{REC}}) = \sum_{i=1}^{n} \eta_{COIL,i} \end{cases}. \tag{14}$$

D. Load Transformation

$\mathbf{Z_{REC}}$ is determined by the following circuits after the RX coils. As shown in Fig. 4, a rectifier and a dc/dc converter are usually added after each RX coil to achieve ac/dc conversion and output voltage regulation. In this paper $R_{DC,i}$ and $R_{L,i}$ are defined as the input resistance of the dc/dc converter and the actual load. $\mathbf{R_{DC}}$ and $\mathbf{R_L}$ are the vectors for $R_{DC,i}$'s and $R_{L,i}$'s respectively.

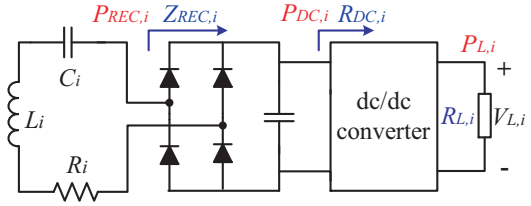

Fig. 4. Configuration of each receiver.

At MHz, $Z_{REC,i}$ $(= R_{REC,i} + jX_{REC,i})$ is no longer a pure resister. [28] has evaluated the relationship between $Z_{REC,i}$ and $R_{DC,i}$, which is shown in Fig. 5. According to the curves of $R_{REC,i}$ and $X_{REC,i}$, a linear model can be used to represent $Z_{REC,i}$ when $R_{DC,i}$ is not too large,

$$Z_{REC,i} = R_{REC,i} + jX_{REC,i} = (\alpha + j\beta)R_{DC,i}, \tag{15}$$

where α and β are constant coefficients and can be obtained from Fig. 5. (15) implies that tuning $Z_{REC,i}$ can be equivalently achieved by adjusting $R_{DC,i}$. A practical application usually uses the dc/dc converter to control $R_{DC,i}$. Here a buck converter is used and it has

$$R_{DC,i} = \frac{R_{L,i}}{D_i^2} = \frac{V_{L,i}^2}{P_{L,i} D_i^2}, \tag{16}$$

where D_i is the duty cycle.

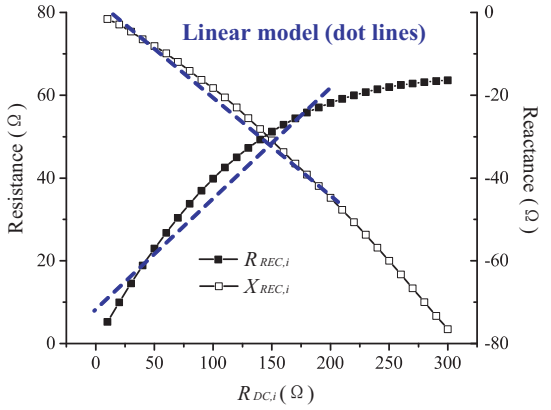

Fig. 5. Rectifier input impedance at 6.78 MHz.

In the proposed system configuration, four power stages (dc/ac, ac/ac, ac/dc, and dc/dc) are included and the efficiency of each stage can be affected by the final loading condition. However, the load sensitivity of each stage is quite different. Usually, the PA and the coupling coils are much more sensitive to loads than the rectifier and the buck converter [6]. Therefore, the efficiency of the rectifier $\eta_{REC,i}$ and the buck converter $\eta_{DC,i}$ can be treated as constants to simplify the model and analysis. Then the power received by $R_{L,i}$ and the efficiency from the PA to $R_{L,i}$ are

$$\begin{cases} P_{L,i}(V_{PA}, \mathbf{R_{DC}}) = P_{REC,i} \cdot \eta_{REC,i} \cdot \eta_{DC,i} \\ \eta_{SYS,i}(\mathbf{R_{DC}}) = \eta_{PA} \cdot \eta_{COIL,i} \cdot \eta_{REC,i} \cdot \eta_{DC,i} \end{cases}. \tag{17}$$

The overall output power (received by $\mathbf{R_L}$) and system efficiency are

$$\begin{cases} P_L(V_{PA}, \mathbf{R_{DC}}) = \sum_{i=1}^{n} P_{L,i} \\ \eta_{SYS}(\mathbf{R_{DC}}) = \sum_{i=1}^{n} \eta_{SYS,i} \end{cases}. \tag{18}$$

Therefore, $\mathbf{R_{DC}}$ and V_{PA} can be designed as two control variables for power and efficiency control. It shows that the power is affected by both $\mathbf{R_{DC}}$ and V_{PA}, and that efficiency is only affected by $\mathbf{R_{DC}}$. The power and efficiency are closely coupled through $\mathbf{R_{DC}}$. Given V_{PA}, it should have a $\mathbf{R_{DC}}$ to fulfill the power requirement, and the corresponding η_{SYS} can then be determined. Theoretically, the choice for V_{PA} could be infinite, and the proposed control approach should quickly tune V_{PA} to optimize η_{SYS} when constant $V_{L,i}$ is maintained.

E. One-RX Model

In a n-RX system, there are at least (n+1) objectives for power and efficiency control, and all these objectives are closely related. Therefore, the known coupling variation effects discussed in one-RX systems can hardly be applied for multiple-RX systems, which further increases the control difficulty. In order to simplify the complexity, it is important to develop proper modeling approach. In such a complicated system, the variation of each RX can all be seen by the TX. Thus it is possible to view all the RXs as an equivalent RX, and then the overall power-efficiency characteristics can be evaluated.

A one-RX model is developed based on the analytical discussion. In this model, $R_{DC,EQ}$ and M_{EQ} are defined as the input resistance of the buck converter and mutual inductance, respectively. This equivalent one RX should provide the same loading effect as that of all the real RXs, which means the same reflected impedance at the TX side [refer to Fig. 3 and (11)]. In real applications, it usually has $Z_{REC,i} \gg R_i$, i.e., a neglectable R_i. Taking (15) into (11), the same overall reflected impedance can then be achieved by equaling the sum of real $Z_{R,i}$'s to the reflected impedance of the equivalent one RX, i.e.,

$$\sum_{i=1}^{n} Z_{R,i} = \sum_{i=1}^{n} \frac{\omega^2 M_{ti}^2}{(\alpha + j\beta) R_{DC,i}} = \frac{\omega^2 M_{EQ}^2}{(\alpha + j\beta) R_{DC,EQ}}. \tag{19}$$

A sufficient condition for (19) is

$$\begin{cases} R_{DC,EQ} = R_{DC,1} \parallel R_{DC,2} \parallel \cdots \parallel R_{DC,n} \\ {M_{EQ}}^2 = \sum_{i=1}^{n} \frac{R_{DC,EQ}}{R_{DC,i}} {M_{ti}}^2 \end{cases}. \tag{20}$$

In this model, $R_{DC,EQ}$ is a parallel combination of all $R_{DC,i}$'s, which is straightforward. However, M_{EQ} cannot be obtained if $\mathbf{M}$ (real coupling) is unknown. Although it is impractical to exactly measure $\mathbf{M}$ for real-time control, it is possible to predict the variation range of $\mathbf{M}$ by defining the wireless charging area. Define M_{MAX} and M_{MIN} as the maximum and minimum values of M_{ti}. Then the variation range of M_{EQ} can be determined based on (20),

$$\begin{cases} {M_{EQ}}^2 \geq \sum_{i=1}^{n} \frac{R_{DC,EQ}}{R_{DC,i}} {M_{MIN}}^2 = {M_{MIN}}^2 \\ {M_{EQ}}^2 \leq \sum_{i=1}^{n} \frac{R_{DC,EQ}}{R_{DC,i}} {M_{MAX}}^2 = {M_{MAX}}^2 \end{cases}, \tag{21}$$

namely,

$$M_{EQ} \in [M_{MIN}, M_{MAX}]. \tag{22}$$

It is interesting to note that the variation range of this equivalent coupling is exactly the same as that of the real coupling. But there are still obvious differences between the real coupling and equivalent one. For example, the real coupling has exact physical meaning and can only be affected by the coil position. However, in a multiple-RX system, the system uncertainties are mainly caused by the changes of $\mathbf{R_L}$, $\mathbf{M}$, and the number of RXs. All these factors can lead to the variation of M_{EQ}. It also means the complicated variations can be combined and studied through a single variable. Thus the system complexity can be largely reduced. From an overall perspective, the system should fulfill the power requirements and maintain high efficiency when M_{EQ} is varied in $[M_{MIN}, M_{MAX}]$. This final objective for multiple-RX systems is quite similar to that of a real one-RX system.

In this paper, the final control objectives are the output voltages and overall efficiency. It is ineffective to directly represent the n-dimension voltages in a one-RX model. Since there is a nature relationship between power, voltage, and load resistance ($P = V^2/R$), the output power of each RX ($P_{L,i}$) can be uniquely determined with given load resistance, and then the overall output power is obtained accordingly. This overall output power has real physical meaning and can be directly represented in the one-RX model. Using the overall power instead of the voltages, the system dimension can be dramatically decreased. This helps to reduce the difficulty in the following analysis.

III. Power and Efficiency Control

The received power ($P_{L,i}$'s) and overall efficiency (η_{SYS}) are closely coupled issues and can be controlled through tuning $\mathbf{R_{DC}}$ and V_{PA} [refer to (18)]. Therefore, there are (n+1) control variables for (n+1) objectives. In order to simplify the control complexity, the challenge is to develop a design and control scheme through which the objectives can be achieved using independent controllers. The proposed one-RX model is applied to discuss the system design and control approaches.

The system parameters are shown in Table I, which are as same as the ones in the following experiment. Here briefly reviews the classical design process of the PA [26]. The maximum input voltage V_{PA} is set at 30V, and the voltage stress on S_1 ($\approx 3.6V_{PA}$) can be estimated as 110 V. Thus a 150 V device is selected. The maximum output power of the PA is designed as 20 W. Taking $P_{COIL} = 20W$ and $V_{PA} = 30V$ into (3) can plot a figure such as Fig. 2 (b), and then Z_{OPT} is found to be 15 Ω. Finally, Z_{OPT} is used to calculate B and X (i.e., C_S, L_0 and C_0) according to (2). In the proposed system, all kinds of variation caused by the load resistance, real coupling, and number of RXs can lead to a varied reflected impedance at the TX side and significantly affect the PA performance. The proposed system model is based on the classical PA model, which fully considers all the above issues [refer to (3)].

TABLE I
System Parameters in Simulation.

Z_{OPT}	B	X	R_t	R_i	M_{MIN}
15 Ω	0.012	17.3	1.50 Ω	0.65 Ω	0.30 μH
M_{MAX}	α	β	$\eta_{REC,i}$	$\eta_{DC,i}$	$R_{L,i}$
0.60 μH	0.32	0.22	95%	90%	10 Ω

A. Power Control With Fixed M_{EQ}

This section is to develop the power control method when M_{EQ} is fixed. $P_{L,TAR}$ is defined as the overall power requirements and

$$P_{L,TAR} = \sum_{i=1}^{n} P_{L,TAR,i}, \tag{23}$$

where $P_{L,TAR,i}$ is the required power for RX_i to keep $V_{L,i}$ constant. This general definition for $P_{L,TAR}$ can cover all the power variation conditions, such as the change of load resistance and number of RXs. From an overall perspective, a system can be stable only if $P_{L,TAR}$ can be fulfilled.

1) PI-Based RX Controller: Using Table I, an example two-RX system can be built with $M_{t1} = M_{t2} = M_{EQ} = 0.6\mu$H and $V_{PA} = 20V$. Since the coupling is known, the overall power-efficiency characteristics be exactly evaluated through its one-RX model. As shown in Fig. 6, assume $P_{L,TAR,1} = P_{L,TAR,2} = 5W$ and $P_{L,TAR} = 10W$, and then this system can achieve stable state at point A or B. In these two monotonic regions (divided by the power peak $R_{DC,P}$), a PI-controller can be used for each RX to achieve independent power control. For example, a system is originally stable at point A. When $P_{L,TAR,1}$ increases from 5 W to 6 W with $P_{L,TAR,2}$ unchanged, $P_{L,TAR}$ becomes 11 W [refer to the green dot line in Fig. 6]. In order to keep $V_{L,1}$ constant, $R_{DC,1}$ is automatically reduced to receive more power. Smaller $R_{DC,1}$ can then lead to smaller $R_{DC,EQ}$ ($R_{DC,EQ} = R_{DC,1}||R_{DC,2}$) and larger output power capability. During this process, although RX_2 will be affected by RX_1, $R_{DC,2}$ can also be tuned independently to keep $V_{L,2}$ constant based on the same mechanism. Finally, the independent PI-based controller of each RX can lead the whole system to achieve a new stable state (point A').

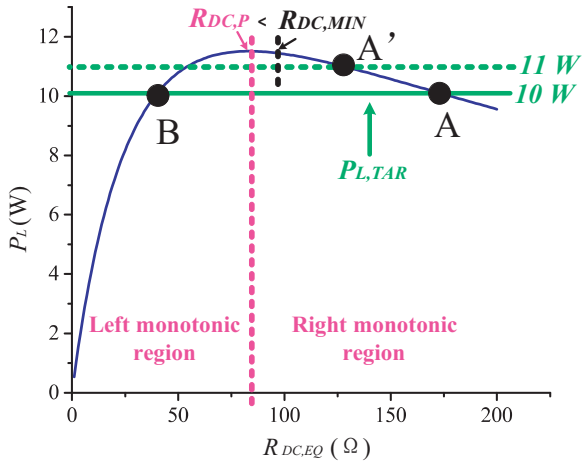

Fig. 6. P_L versus $R_{DC,EQ}$ with fixed M_{EQ}.

2) Monotonic Region Selection: In order to use the independent PI controller, all RXs and the whole system should keep working in one of the monotonic regions. However, the left region is not suitable because the RXs cannot be disabled (i.e., receiving no power). For example, in the left region, the output power increases with the load resistance. A RX can be disabled only by providing zero $R_{DC,i}$. However, zero $R_{DC,i}$ will lead to zero $R_{DC,EQ}$ and completely change the overall output power capability. As a result, all the other RXs will fail in receiving power no matter how their controllers tune. The right monotonic region does not have this concern. In this region, a RX can be disabled by providing infinite $R_{DC,i}$. Once a specific $R_{DC,i}$'s becomes infinite, it will lead to smaller $R_{DC,EQ}$. Finally, the overall output power decreases and a new stable state is still achievable. In practice, defining

$R_{DC,MIN}$ as the minimum $R_{DC,EQ}$, and then choosing

$$R_{DC,P} < R_{DC,MIN} \tag{24}$$

can leave a safety margin to avoid the PI control jumping into the left region [refer to Fig. 6]. Overall, the right monotonic region is suitable for systems with independent PI-based RX controllers.

B. Power Control With Varied M_{EQ}

In practice, a device can be randomly placed on the charging board within a defined area, and it is ineffective to measure the coupling in a real-time manner for control purpose. However, it is possible to tune the system within a known coupling variation range. This section discusses the design methodology for V_{PA} such that the proposed independent RX controller can be applied in a system with coupling varied in a known range. Table I defines such a system. Using the proposed one-RX model, the overall power-efficiency characteristics can be predicted, as shown in Fig. 7. Since the variation range of the real coupling is known, M_{EQ} is determined accordingly. When $V_{PA} = 20V$, all the changes of $\mathbf{R_L}$, $\mathbf{M}$, and the number of RXs can be reflected by the varied M_{EQ} in the known range. Although the system performance cannot be known exactly like a fixed M_{EQ} case, the boundary of the performance can be determined by the cases with minimum and maximum M_{EQ} [refer to the black and blue curves in Fig. 7].

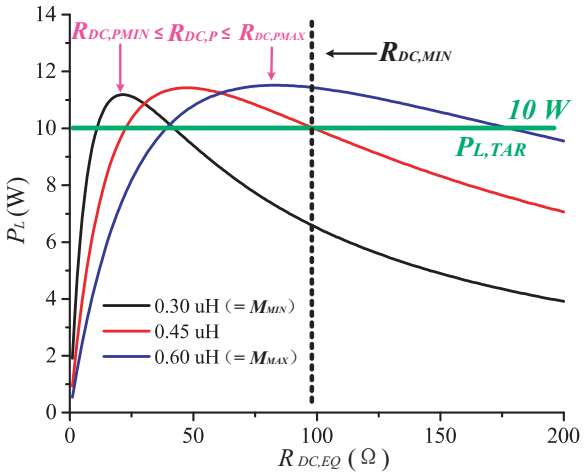

Fig. 7. P_L versus $R_{DC,EQ}$ under varied M_{EQ}.

1) Staying in the Right Monotonic Region: In the fixed M_{EQ} case, the independent RX controller can work only if the system keeps operating in the right monotonic region [refer to Fig. 6]. Similarly, the system should always operate in the right region under varied M_{EQ}. The boundary of monotonic region is the peak point ($R_{DC,P}$) of these curves, and $R_{DC,P}$ is moving within a range as shown in Fig. 7, i.e.,

$$R_{DC,PMIN} \le R_{DC,P} \le R_{DC,PMAX}. \tag{25}$$

In order to keep operating in the right region, $R_{DC,MIN}$ should be larger than $R_{DC,PMAX}$, i.e.,

$$R_{DC,PMAX} < R_{DC,MIN} \le R_{DC,EQ}. \tag{26}$$

Note that $R_{DC,PMAX}$ does not depend on V_{PA}, and it means $R_{DC,MIN}$ can be designed as a constant once the system parameters are known.

2) Determination of $V_{PA,MIN}$: A system can always achieve a stable state when V_{PA} is sufficiently large. Therefore, there exists a minimum V_{PA}, defined as $V_{PA,MIN}$, to fulfill a specific power requirement $P_{L,TAR}$. Since $R_{DC,MIN}$ is determined by the system parameters as shown in Fig. 7, the objective here is to determine $V_{PA,MIN}$ based on $P_{L,TAR}$ and $R_{DC,MIN}$.

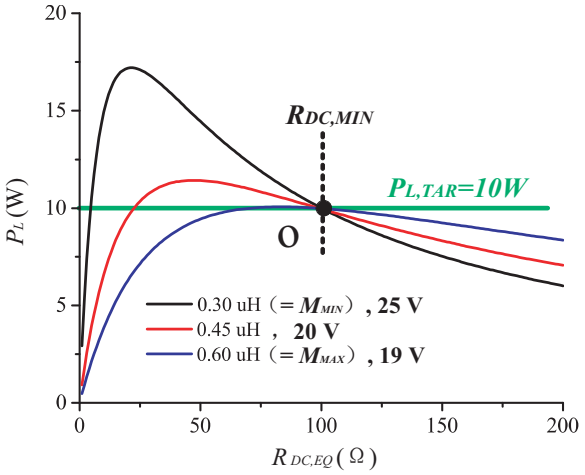

Fig. 8. The minimum required V_{PA} for different M_{EQ} when $R_{DC,EQ} \in [R_{DC,MIN}, +\infty]$.

An example is shown in Fig. 8, which uses the same parameters as those in Fig. 7. For any M_{EQ}, P_L decreases with the increasing R_{EQ} in the right monotonic region. It means P_L is maximized at $R_{DC,MIN}$ for any given V_{PA}. Define point O as the intersection of the constant $R_{DC,MIN}$ and the constant $P_{L,TAR}$. The minimum V_{PA} for a maximum M_{EQ} case can be obtained by increasing V_{PA} from zero until the blue line passing the point O. Similar process can be applied to the other coupling cases. As shown in Fig. 8, the overall system $V_{PA,MIN}$ is determined by the minimum M_{EQ} case, i.e., $M_{EQ} = 0.30\mu$H, choosing $V_{PA,MIN} = 25V$ can make system achieve stable state under varied M_{EQ}. Mathematically, $V_{PA,MIN}$ is the solution of

$$P_L(V_{PA,MIN}, R_{DC,MIN}) = P_{L,TAR}, \tag{27}$$

when $M_{EQ} = M_{MIN}$. Since $R_{DC,MIN}$ is determined by M_{MAX}, it is interesting to note that $V_{PA,MIN}$ is actually determined by both M_{MAX} and M_{MIN}. In real application, the varied power caused by the loads or the number of RXs can all lead to a varied $P_{L,TAR}$, which further determines $V_{PA,MIN}$. By having $V_{PA} \ge V_{PA,MIN}$, the system can ensure sufficient output power ability and all RXs can always work independently in the right monotonic region. Although power characteristics are uncertain in a range, the voltage tuning mechanism for varied M_{EQ} case is exactly the same as that of fixed M_{EQ} case [refer to the automatic tuning from point A to point A' in Fig.6].

C. Optimizing Efficiency

This subsection explains the control of V_{PA} within the range of $[V_{PA,MIN}, +\infty]$ for efficiency optimization. Using the same system parameters, Fig. 9 gives P_L and η_{SYS} for $V_{PA} = 20V$. $R_{DC,E}$ is the efficiency peak. Similar to the uncertain power peak $R_{DC,P}$, it has $R_{DC,E} \in [R_{DC,EMIN}, R_{DC,EMAX}]$ when $M_{EQ} \in [M_{MIN}, M_{MAX}]$. Since η_{SYS} does not depend on V_{PA} [refer to (18)], V_{PA} has none effects on $R_{DC,E}$. For different M_{EQ}, the efficiency peak is always located at the left of the power peak, i.e.,

$$R_{DC,E} < R_{DC,P} < R_{DC,MIN} \leq R_{DC,EQ} \tag{28}$$

Thus the efficiency increases with the decreasing $R_{DC,EQ}$ and is maximized at minimum $R_{DC,EQ}$. To achieve a stable state, $R_{DC,EQ}$ decreases with V_{PA} [refer to Fig.8]. Therefore, η_{SYS} is maximized at the minimum V_{PA}, i.e., $V_{PA,MIN}$.

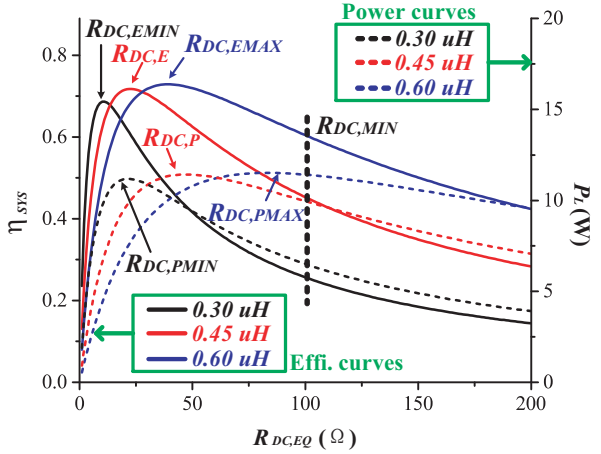

Fig. 9. P_L and η_{SYS} versus $R_{DC,EQ}$ when $M_{EQ} \in [0.30, 0.60]\mu H$ and $V_{PA} = 20V$.

$V_{PA} = V_{PA,MIN}$ can only optimize the efficiency under the constrain designed for the independent working of RX controllers. This optimized efficiency is not the global one. If the global optimum efficiency has to be achieved, the linear PI controller cannot be used due to the nature of the parabola power curves. A n-dimensional tracking method could be applied, which greatly increases the control complexity. There is always a trade-off between the power control complexity and optimized efficiency. In small-power applications, a stable output voltage with simple circuit is usually more desirable than the system efficiency.

Although the proposed method cannot achieve global optimum efficiency, it can be designed close to it by limiting the variation range of real coupling. Fig. 9 is an example system with a large difference between M_{MAX} and M_{MIN}. The optimized efficiency is determined by the distance between $R_{DC,MIN}$ and $R_{DC,E}$. If all the real couplings are fixed with $M_{ti} = M_{EQ} = M_{MIN} = M_{MAX} = 0.60\mu$H, $R_{DC,EMAX}$ becomes the real efficiency peak and gets closer to $R_{DC,MIN}$. It means the optimized efficiency is improved. Therefore, a small coupling variation range is desired.

D. Summery and System Control Block

The basic idea of the system design and control is summarized in Fig. 10. The objective is to fulfill all RXs' power requirements with an optimal η_{SYS} when M_{EQ} is uncertain within $[M_{MIN}, M_{MAX}]$. In a fixed M_{EQ} case, two monotonic regions exist for power control. Only the right one can be used to ensure the independence of each PI-based RX controller. When M_{EQ} is uncertain, $R_{DC,EQ} \geq R_{DC,MIN} > R_{DC,PMAX}$ should be satisfied to make sure the system can keep operating in the right region. $V_{PA,MIN}$ is then determined based on $R_{DC,MIN}$ for a specific $P_{L,TAR}$. With the derived $V_{PA,MIN}$, the system can naturally reach a stable state by applying the simple PI-based control for each RX. After obtaining the range of V_{PA}, the next step is to optimize η_{SYS} by tuning V_{PA}. The relationship between the peaks of P_L and η_{SYS} in (28) infers the maximum efficiency occurs on the constrain boundary, i.e., when $V_{PA} = V_{PA,MIN}$. Therefore, a look-up table can be used in the TX controller to optimize the overall efficiency.

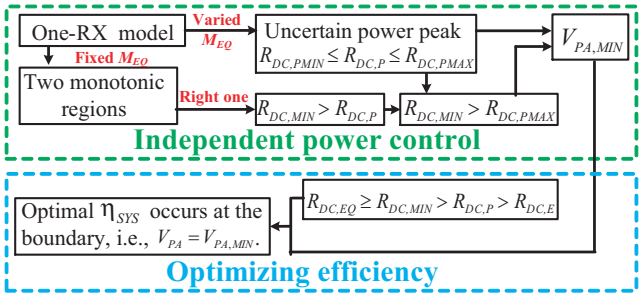

Fig. 10. Design flow chart.

The system control diagram is shown in Fig. 11, which consists of one TX and n RXs. The TX coil is driven by the Class E PA [see Section II-B], whose input voltage V_{PA} can be tuned by the TX controller. For each RX, it includes a RX coil, a rectifier, a buck converter, and a RX controller. Each RX uses a PI controller to provide a constant $V_{L,TAR,i}$. Through wireless communication, all required $P_{L,TAR,i}$'s can be sent to TX controller to obtain $P_{L,TAR}$. Then the TX controller tunes V_{PA} according to the look-up table. Note the proposed methodology is suitable for MHz WPT systems such as working at 6.78 or 13.56 MHz. However, if the frequency is further increased (such as 27.12 MHz), the bridge rectifier may fail and the methodology becomes invalid.

IV. Experimental Verification

A. Experiment setup

A three-RX 15W WPT system is built up in the final experiment as shown in Fig. 12(a), which has exactly the same configuration as Fig. 11. At the TX side, a programmable dc source is used to provide V_{PA} for a 6.78 MHz Class E PA, and a TX coil is driven by the PA [see Fig. 12 (b)(c)]. A computer is used as the TX controller, and it can directly communicate with the dc source and adjust V_{PA}. Each RX consists of a RX coil, a rectifier, a buck converter, a I/V sampling board, a RX controller (NI myRIO), and an electronic load. The

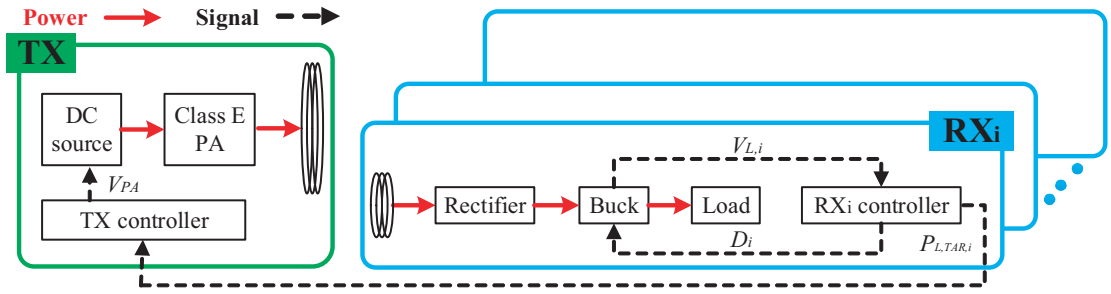

Fig. 11. System control block diagram.

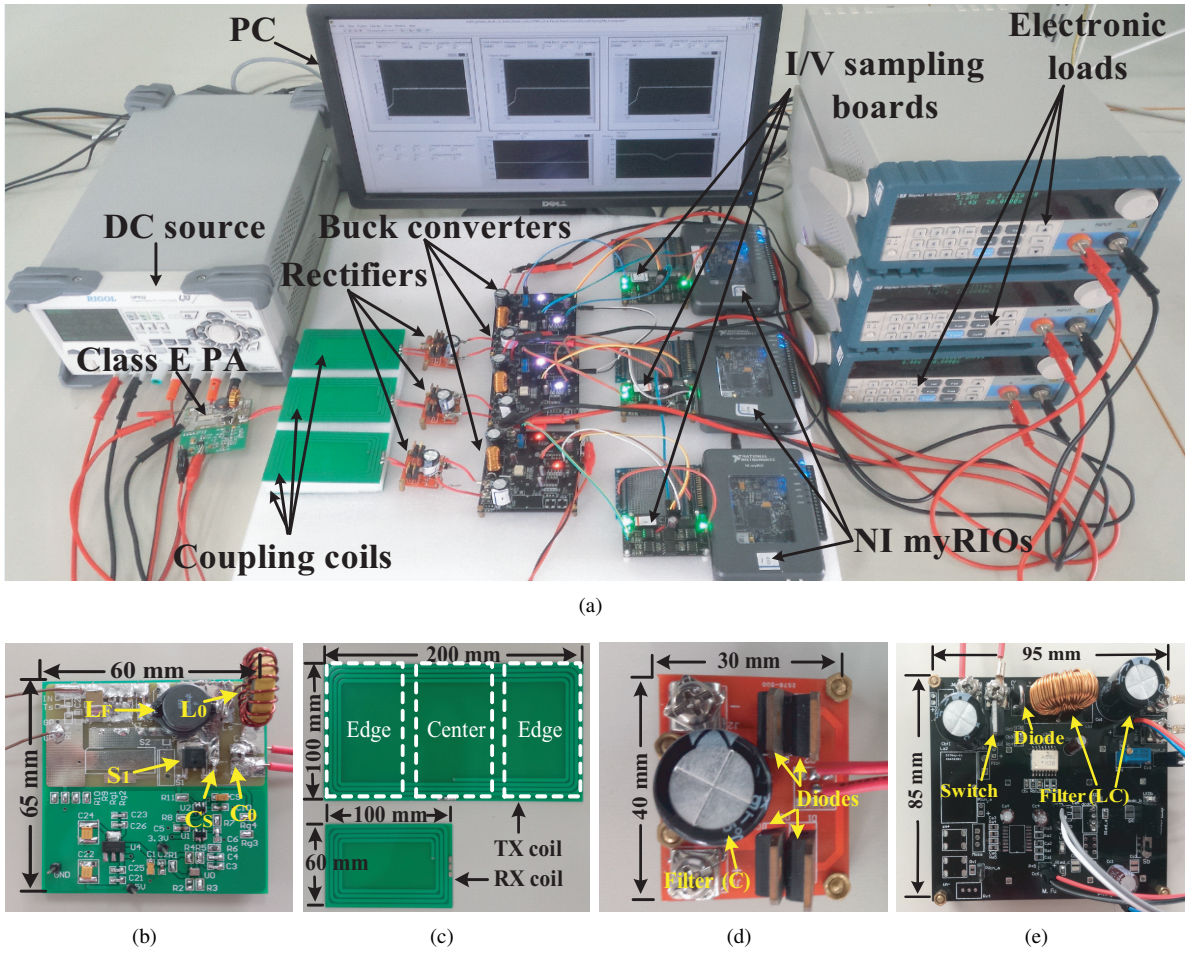

Fig. 12. Experiment setup. (a) Overview. (b) Class E PA. (c) Coupling Coils. (d) Rectifier. (e) Buck converter.

output voltage $V_{L,i}$ and current $I_{L,i}$ can be measured by the RX controller. All the RX controllers can communicate with the TX controller through WiFi. The coil layout is illustrated in Fig. 12 (c). The three identical RX coils are placed right above the TX coil, as shown in Fig. 12 (a). Again, RX coil overlap is not allowed and cross coupling among RX coils can be ignored. The vertical distance between RX coils and TX coil is 20 mm. Such a placement can give a small range of M_{EQ}, and usually the center one (RX_2) has the largest coupling and the other two (RX_1 and RX_3) have the smallest. All the system parameters are summarized in Table II. Note the PA's parameters are designed according to B and X in Table I.

TABLE II
PARAMETERS OF PA AND COUPLING COILS.

S_1	L_F	C_S	L_0	C_0	L_t
SUD06N150	$68\mu H$	287pF	$1.47\mu H$	523pF	$5.40\mu H$
$[M_{MIN}, M_{MAX}]$	C_t	R_t	L_i	C_i	R_i
$[0.48\mu H, 0.51\mu H]$	104pF	1.50Ω	$1.89\mu H$	292pF	0.65Ω

B. Designing $R_{DC,MIN}$ and $V_{PA,MIN}$

The experiment should follow the methodology in Section III to obtain $R_{DC,MIN}$ and $V_{PA,MIN}$. Open-loop tests can

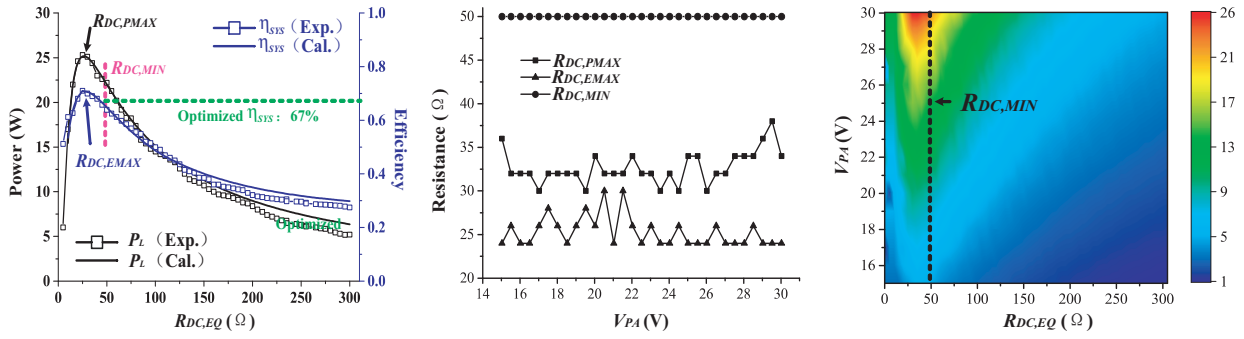

(a) (b) (c)

Fig. 13. System output characteristics. (a) Comparison between calculation and experiment. (b) $R_{DC,PMAX}$ and $R_{DC,EMAX}$ under different V_{PA}. (c) P_L under different V_{PA} and $R_{DC,EQ}$ when $M_{EQ} = M_{MIN}$.

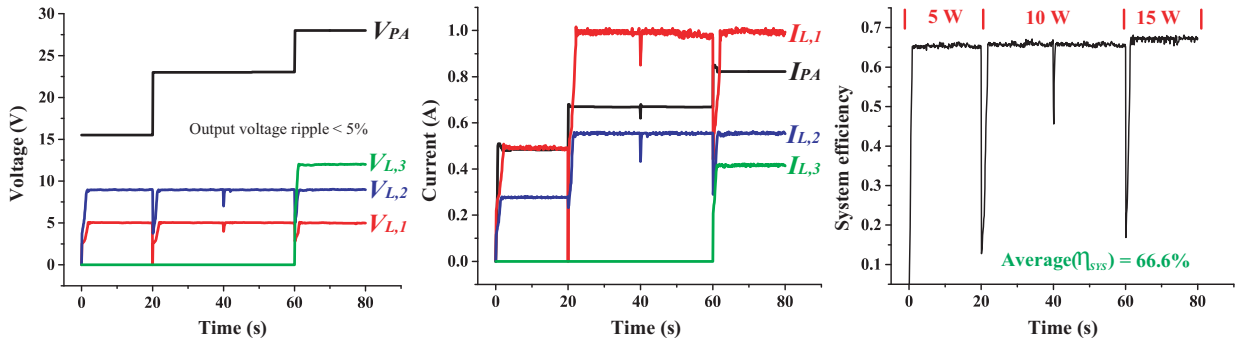

(a) (b) (c)

Fig. 14. System dynamic response. (a) Input and output voltages. (b) Input and output currents. (c). System overall efficiency η_{SYS}.

be first conducted to obtain $R_{DC,MIN}$. Since $R_{DC,MIN}$ is determined by the maximum M_{EQ}, only one RX is placed in the center position to guarantee $M_{EQ} = M_{MAX}$ [refer to Fig. 12(c)]. The load resistance is fixed at 10 Ω and the sweeping of $R_{DC,EQ}$ is achieved by changing the duty cycle of the buck converter. Therefore, the measured output power and efficiency cover all four stages. Fig. 13(a) gives the output power and efficiency for $V_{PA} = 30V$. The experiment (exp.) results are shown to be consistent with the calculation (cal.) results, especially around the power and efficiency peaks. Due to the constant-efficiency assumption for η_{BUCK}, the error becomes larger when $R_{DC,EQ}$ is large. However, this error does not affect the control because only the characteristics around peaks are used to design the system. Similar tests are further carried out for more V_{PA}'s, and all the power and efficiency peaks, i.e., $R_{DC,PMAX}$ and $R_{DC,EMAX}$, are abstracted and summarized in Fig. 13 (b). It shows $R_{DC,PMAX} > R_{DC,EMAX}$ for all V_{PA}'s, which is consistent with (28). Also it shows V_{PA} has little influence over on these peaks as the analytical model predicts. Based on these results, $R_{DC,MIN}$ is designed as 50 Ω to ensure $R_{DC,MIN} > R_{DC,PMAX}$. Considering the small perturbation of PI controllers, a safety margin is also left [refer to (26)]. All the above design considerations follow the conclusions made from Fig. 6-7.

After obtaining $R_{DC,MIN}$, the next step is to get $V_{PA,MIN}$ for different $P_{L,TAR}$. The required condition, $M_{EQ} = M_{MIN}$, is achieved by placing one RX at the edge position [refer to Fig. 12(c)]. The system output power is then measured for different $R_{DC,EQ}$ and V_{PA}, as shown in Fig. 13 (c). In this figure, drawing a line at $R_{DC,EQ} = R_{DC,MIN}$ can give a look-up table of $V_{PA,MIN}$ for different $P_{L,TAR}$ [refer to (27)]. Finally, a dot line for $R_{DC,EQ} = R_{DC,MIN}$ can also be plotted in Fig. 13 (a). In order to ensure the independent voltage regulation for each RX controller, $R_{DC,EQ} \geq R_{DC,MIN}$ should be guaranteed by having sufficiently large input voltage, i.e., $V_{PA} \geq V_{PA,MIN}$. When $V_{PA} = V_{PA,MIN}$, η_{SYS} (about 67%) is optimized at $R_{DC,MIN}$.

C. Dynamic Response Under Varied M_{EQ}

In this experiment, all the controllers are enabled to give a close-loop test of the proposed control approach. The full power of each receiver is 5 W but with different target voltages ($V_{L,TAR,1} = 5V$, $V_{L,TAR,2} = 9V$, and $V_{L,TAR,3} = 12V$). Therefore, the full power of this three-RX system is 15 W. During this experiment, the system response is recorded under all kinds of variations caused by the load resistance, real coupling, and number of RXs. Four periods are designed and each period lasts for 20 s.

Fig. 14 (a)(b) gives the system response for the input and output voltages and currents, respectively. At the first period (0-20 s), RX_1 and RX_2 are placed at the edges with half load condition (i.e., $P_{L,TAR,1} = P_{L,TAR,2} = 2.5$ W). So $P_{L,TAR}$ is 5 W. V_{PA} is controlled at 15.5V based on the look-up table abstracted from Fig. 13 (c). Fig. 14 (a) shows $V_{L,1}$ and $V_{L,2}$ can achieve the target voltage with a fast response.

TABLE III
COMPARISON OF 6.78 MHZ WPT SYSTEMS FOR PLANAR CHARGING APPLICATION.

Ref.	Coil Size (mm)	d (mm)	Num. of RX	Power Stages	Efficiency	Output
[16]	TX:180×180, RX:47×47	12	4	ac/ac	Peak: 93%	Unregulated
[29]	TX:125×89;RX:71×57	25	1	dc/ac, ac/ac, ac/dc	Peak:78%	Unregulated
[24]	TX:200×100, RX:100×60	20	3	dc/ac, ac/ac, ac/dc, dc/dc	Avg: 71.7%	Unregulated
[25]	TX:226×116, RX:73×55	8	3	dc/ac, ac/ac, ac/dc, dc/dc	Peak: 66%	Regulated
This work	TX:200×100 , RX:100×60	20	3	dc/ac, ac/ac, ac/dc, dc/dc	Avg.: 66.6%	Regulated

The current response in Fig. 14 (b) is similar to the voltage response because of the use of constant $R_{L,i}$. At t = 20 s, both RXs double the power requirement from half load to full load ($P_{L,TAR} = 10W$). V_{PA} is improved to 23 V by the TX controller. Similar voltage and current responses can be observed. At t = 40 s, RX_2 is moved from the edge to the center while RX_1 is fixed, and both still work at full load condition. It clearly shows that the variation caused by RX_2 can affect RX_1 but the controllers can still work independently. In the last period, RX_3 is added to the edge at t = 60 s. All the RXs work at the full load condition ($P_{L,TAR} = 15W$). It shows the system can work well when adding new RXs. These results can well validate the proposed voltage regulation approach.

Fig. 14 (c) gives the real-time overall efficiency. The average η_{SYS} is 66.6% during the whole period. This value is consistent with the optimized η_{SYS} in Fig.13(a). It means that the tuning of V_{PA} can well optimize the overall system efficiency under all kinds of variations. The results in this paper are compared with the results in other published papers discussing 6.78 MHz systems in Table III. All these systems are developed for small-power planar charging applications with single TX coil. The efficiency of [16] is the highest because only the coil efficiency is considered. Generally, the efficiency becomes lower when more power stages are included. In practice, three stages (dc/ac, ac/ac, and ac/dc) are indispensable for an overall dc/dc conversion. Such kind of system can usually achieve the peak efficiency at a specific position or load resistance [29]. By using dc/dc converters, the system in [24] can track the global maximum efficiency without output voltage regulation. So the efficiency is higher than that of this paper. The dc/dc converters in [25] are used for voltage regulation. However, the peak efficiency 66% measured at full load (15W) drops to 48% at a light load condition (5W). Thanks to the efficiency optimization, η_{SYS} in this paper can be maintained at about 66% over a wide load range [refer to Fig. 14 (c)].

V. CONCLUSION

This paper provides a comprehensive analysis on a MHz multiple-RX system driven by a Class E PA. A novel one-RX model is built to investigate the overall power-efficiency characteristics. In this model, all the variations caused by real coupling, loading, and number of RXs, are represented by the varied equivalent coupling. Thus the system is greatly simplified. Based on this model, independent PI controllers are designed at the RX side for output regulation, and the input voltage is tuned to optimize the overall efficiency at the TX side. The proposed control scheme can be easily implemented and directly applied for commercial electronic devices. Experimental results show that the proposed method can provide different constant output voltages for different receivers. The system efficiency can be maintained above 63% when the number of RXs changes.

REFERENCES

[1] S. Aldhaher, P. C. Luk, and J. F. Whidborne, "Tuning class E inverters applied in inductive links using saturable reactors," *IEEE Trans. Power Electron.*, vol. 29, no. 6, pp. 2969–2978, Jun. 2014.

[2] S. Aldhaher, P. Luk, K. E. K. Drissi, and J. Whidborne, "High-input-voltage high-frequency class E rectifiers for resonant inductive links," *IEEE Trans. Power Electron.*, vol. 30, no. 3, pp. 1328 – 1335, Mar. 2015.

[3] S. Y. R. Hui, W. Zhong, and C. K. Lee, "A critical review of recent progress in mid-range wireless power transfer," *IEEE Trans. Power Electron.*, vol. 29, no. 9, pp. 4500–4511, Sep. 2014.

[4] Y. H. Sohn, B. H. Choi, E. S. Lee, G. C. Lim, G.-H. Cho, and C. T. Rim, "General unified analyses of two-capacitor inductive power transfer systems: Equivalence of current-source SS and SP compensations," *IEEE Trans. Power Electron.*, vol. 30, no. 11, pp. 6030–6045, Nov. 2015.

[5] T. C. Beh, M. Kato, T. Imura, S. Oh, and Y. Hori, "Automated impedance matching system for robust wireless power transfer via magnetic resonance coupling," *IEEE Trans. Ind. Electron.*, vol. 60, no. 9, pp. 3689–3698, Sep. 2013.

[6] M. Fu, H. Yin, X. Zhu, and C. Ma, "Analysis and tracking of optimal load in wireless power transfer systems," *IEEE Trans. Power Eletron.*, vol. 30, no. 7, pp. 3952–3963, Jul. 2015.

[7] M. Fu, T. Zhang, C. Ma, and X. Zhu, "Efficiency and optimal loads analysis for multiple-receiver wireless power transfer systems," *IEEE Trans. Microw. Theory Techn.*, vol. 63, no. 3, pp. 801–812, Mar. 2015.

[8] S. Kong, B. Bae, D. H. Jung, J. J. Kim, S. Kim, C. Song, J. Kim, and J. Kim, "An investigation of electromagnetic radiated emission and interference from multi-coil wireless power transfer systems using resonant magnetic field coupling," *IEEE Trans. Microw. Theory Techn.*, vol. 63, no. 3, pp. 833–845, Mar. 2015.

[9] M. Fu, T. Zhang, X. Zhu, P. C.-K. Luk, and C. Ma, "Compensation of cross coupling in multiple-receiver wireless power transfer systems," *IEEE Trans. Ind. Informat.*, vol. 12, no. 2, pp. 474–482, Apr. 2016.

[10] Z. Pantic, K. Lee, and S. M. Lukic, "Receivers for multifrequency wireless power transfer: Design for minimum interference," *IEEE J. Emerg. Sel. Topics Power Electron.*, vol. 3, no. 1, pp. 234–241, Mar. 2015.

[11] W. Zhong and S. Y. R. Hui, "Auxiliary circuits for power flow control in multifrequency wireless power transfer systems with multiple receivers," *IEEE Trans. Power Electron.*, vol. 30, no. 10, pp. 5902–5910, Oct. 2015.

[12] Y. Zhang, T. Lu, Z. Zhao, F. He, K. Chen, and L. Yuan, "Selective wireless power transfer to multiple loads using receivers of different resonant frequencies," *IEEE Power Electron. Lett.*, vol. 30, no. 11, pp. 6001–6005, Nov. 2015.

[13] Y.-J. Kim, D. Ha, W. J. Chappell, and P. P. Irazoqui, "Selective wireless power transfer for smart power distribution in a miniature-sized multiple-receiver system," *IEEE Trans. Ind. Electron.*, vol. 63, no. 3, pp. 1853–1862, Mar. 2016.

[14] K. K. Ean, B. T. Chuan, T. Imura, and Y. Hori, "Impedance matching and power division using impedance inverter for wireless power transfer," *IEEE Trans. Ind. Appl.*, vol. 50, no. 3, pp. 2061–2070, May. 2014.

[15] K. Lee and D.-H. Cho, "Analysis of wireless power transfer for adjustable power distribution among multiple receivers," *IEEE Antennas Wireless Propag. Lett.*, vol. 14, pp. 950–953, Jan. 2015.

[16] J. Kim, D.-H. Kim, and Y.-J. Park, "Free-positioning wireless power transfer to multiple devices using a planar transmitting coil and switchable impedance matching networks," *IEEE Trans. Microw. Theory Techn.*, vol. 64, no. 11, pp. 3714–3722, Nov. 2016.

[17] Y. Zhang, T. Lu, Z. Zhao, K. Chen, F. He, and L. Yuan, "Wireless power transfer to multiple loads over various distances using relay resonators," *IEEE Mirow. Compon. Lett.*, vol. 25, no. 5, pp. 337–339, May. 2015.

[18] Y. Zhang, T. Lu, Z. Zhao, F. He, K. Chen, and L. Yuan, "Employing load coils for multiple loads of resonant wireless power transfer," *IEEE Trans. Power Electron.*, vol. 30, no. 11, pp. 6174–6181, Nov. 2015.

[19] J. J. Casanova, Z. N. Low, and J. Lin, "A loosely coupled planar wireless power system for multiple receivers," *IEEE Trans. Ind. Electron.*, vol. 56, no. 8, pp. 3060–3068, Aug. 2009.

[20] D. Ahn and S. Hong, "Effect of coupling between multiple transmitters or multiple receivers on wireless power transfer," *IEEE Trans. Ind. Electron.*, vol. 60, no. 7, pp. 2602–2613, Jul. 2013.

[21] M. Q. Nguyen, Y. Chou, D. Plesa, S. Rao, and J.-C. Chiao, "Multiple-inputs and multiple-outputs wireless power combining and delivering systems," *IEEE Trans. Power Electron.*, vol. 30, no. 11, pp. 6254–6263, Jun. 2015.

[22] W. M. Ng, C. Zhang, D. Lin, and S. Y. R. Hui, "Two- and three-dimensional omnidirectional wireless power transfer," *IEEE Power Electron. Lett.*, vol. 29, no. 9, pp. 4470–4474, Sep. 2014.

[23] C. Zhang, D. Lin, and S. Hui, "Basic control principles of omnidirectional wireless power transfer," *IEEE Trans. Power Electron.*, vol. 31, no. 7, pp. 5215–5227, Jul. 2016.

[24] M. Fu, H. Yin, and C. Ma, "Megahertz multiple-receiver wireless power transfer systems with power flow management and maximum efficiency point tracking," *IEEE Trans. Microw. Theory Techn.*, 2017, DOI:10.1109/TMTT.2017.2689747.

[25] P. S. Riehl, A. Satyamoorthy, H. Akram, Y.-C. Yen, J.-C. Yang, B. Juan, C.-M. Lee, F.-C. Lin, V. Muratov, W. Plumb *et al.*, "Wireless power systems for mobile devices supporting inductive and resonant operating modes," *IEEE Trans. Microw. Theory Techn.*, vol. 63, no. 3, pp. 780–790, Mar. 2015.

[26] F. H. Raab, "Idealized operation of the class E tuned power amplifier," *IEEE Trans. Trans. Circuits Syst.*, vol. 24, no. 12, pp. 725–735, Dec. 1977.

[27] M. Fu, H. Yin, M. Liu, and C. Ma, "Loading and power control for a high-efficiency class E pa-driven megahertz wpt system," *IEEE Trans. Ind. Electron.*, vol. 63, no. 11, pp. 6867–6876, Jul. 2016.

[28] M. Fu, Z. Tang, M. Liu, C. Ma, and X. Zhu, "Full-bridge rectifier input reactance compensation in megahertz wireless power transfer systems," in *2015 IEEE PELS Workshop on Emerging Technologies: Wireless Power, Daejeon, Korea,*, Jun. 2015, pp. 1–5.

[29] D. Ahn and P. P. Mercier, "Wireless power transfer with concurrent 200-kHz and 6.78-MHz operation in a single-transmitter device," *IEEE Trans. Power Electron.*, vol. 31, no. 7, pp. 5018–5029, 2016.

Minfan Fu (S'13-M'16) received the B.S., M.S., and Ph.D. degrees in electrical and computer engineering from University of Michigan-Shanghai Jiao Tong University Joint Institute, Shanghai Jiao Tong University, Shanghai, China in 2010, 2013, and 2016, respectively.

He is currently a postdoctoral researcher at the Center for Power Electronics Systems, Virginia Polytechnic Institute and State University, Blacksburg, VA, USA. His research interests include megahertz wireless power transfer, high-frequency power conversion, high-frequency magnetic design, and application of wide-band-gap devices.

He Yin (S'13-M'16) received the B.S. degree and Ph.D. degreee in electrical and computer engineering from University of Michigan-Shanghai Jiao Tong University Joint Institute, Shanghai Jiao Tong University, Shanghai, China, in 2012 and 2017, respectively.

He is currently a postdoctoral researcher in the Department of Electrical Engineering & Computer Science, the University of Tennessee, Knoxville. His research interests include optimization and distributed control of networked energy systems such as microgrids and multiple-receiver wireless power transfer systems.

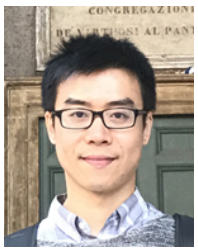

Ming Liu (S'15-M'17) received the B.S. degree from SiChuan University, Sichuan, China, in 2007, the M.S. degree from the University of Science and Technology Beijing, Beijing, China, in 2011, both in mechatronic engineering, and the Ph.D. degree in electrical and computer engineering from University of Michigan-Shanghai Jiao Tong University Joint Institute, Shanghai Jiao Tong University, Shanghai, China, in 2017.

His research interests include high frequency power electronic circuits such as high frequency resonant converters and megahertz wireless power transfer systems, general power electronics and applications, circuit-level and system-level optimization.

Yong Wang (M'05) received his Ph.D. degree in power electronics from Zhejiang University in 2005. After receiving his Ph.D. degree, from 2005-2008, he was a senior researcher in Samsung Advanced Institute of Technology in Korea, researching on the fuel cell grid tied inverter. From 2008-2010, he was working in Danfoss, Denmark, as a power electronics hardware engineer. In 2010, he joined Shanghai Jiao Tong University, Shanghai, China.

Currently he is an associate professor in the Department of Electrical Engineering, Shanghai Jiao Tong University. His main research fields includes wireless charging transfer, multi-level conversion, etc.

Chengbin Ma (M'05) received the B.S. (Hons.) degree in industrial automation from East China University of Science and Technology, Shanghai, China, in 1997, and the M.S. and Ph.D. degrees in electrical engineering from The University of Tokyo, Tokyo, Japan, in 2001 and 2004, respectively.

He is currently an associate professor of electrical and computer engineering at University of Michigan-Shanghai Jiao Tong University Joint Institute, Shanghai Jiao Tong University, Shanghai, China. Between 2006 and 2008, he held a postdoctoral position with the Department of Mechanical and Aeronautical Engineering, University of California Davis, California, USA. From 2004 to 2006, he was a R&D researcher with Servo Laboratory, Fanuc Limited, Yamanashi, Japan. He is an associate editor of the IEEE Transactions on Industrial Informatics. His research interests include networked energy systems, wireless power transfer, and mechatronic control.